Microscopic Study of Tetrahedrally Symmetric Nuclei by Angular-Momentum and Parity Projection Methods

Shingo Tagami and Yoshifumi R. Shimizu

Department of Physics, Faculty of Sciences,

Kyushu University, Fukuoka 812-8581, Japan

Jerzy Dudek

Institut Pluridisciplinaire Hubert Curien (IPHC),

IN_2P_3-CNRS/Université de Strasbourg, F-67037 Strasbourg, France

Abstract

We study the properties of the nuclear rotational excitations with hypothetical tetrahedral symmetry by employing the microscopic mean-field and residual-interaction Hamiltonians with angular-momentum and parity projection method; we focus on the deformed nuclei with tetrahedral doubly-closed shell configurations. We find that for pure tetrahedral deformation the obtained excitation patterns satisfy the characteristic features predicted by group-representation theory applied to the tetrahedral symmetry group. We find that a gradual transition from the approximately linear to the characteristic rigid-rotor, parabolic energy-vs.-spin dependence occurs as a function of the tetrahedral deformation parameter. The form of this transition is compared with the similar well-known transition in the case of quadrupole deformation.

PACS numbers: 21.10.Re, 21.60.Jz, 23.20.Lv, 27.70.+q

I. INTRODUCTION

Symmetries play an important role in physics, often serving as guide-lines in studying characteristic features of motion of quantum systems. In particular, in nuclear physics, the spatial symmetries of the nuclear mean-field potential are crucial in determining both the properties of the independent particle motion and of the nuclear stability. The best known, the spherical symmetry of the potential, implies the high degeneracy of the single-particle level energies, the so-called magnetic degeneracy, $(2j+1)$, of the orbitals characterised by the spherical-shell angular-momentum quantum-number, j, and leads to the well-known spherical magic numbers in nuclei. The spontaneous breaking of the spherical symmetry arises when the energies of the spherical configuration of the system with certain particle numbers are higher as compared to the energies of the alternative non-spherical spatial distribution of nucleons, the mechanism to which the Pauli exclusion principle contributes importantly. The spherical symmetry breaking removes the $(2j+1)$-degeneracy and leads to the deformed single-particle orbital scheme [1, 2].

More generally, nuclei which are not spherical may acquire the forms governed by the point-group symmetries, some being more likely than the others – depending on the actual number of nucleons. In this context, it has been suggested, cf. Ref. [3] and references therein, that each symmetry group 'sufficiently rich' in terms of symmetry elements may lead to its proper scheme of magic numbers, which in turn can be seen as characterising such a symmetry group from the point of view of realistic realisations of the nuclear mean-field theories. In particular, a series of earlier publications related to point-group symmetries focused on the tetrahedral and octahedral symmetry groups which are the only ones that lead to an extra (four-fold) degeneracy of single-nucleonic levels in *deformed* nuclei and to an increased nuclear stability. In other words: The tetrahedral and octahedral symmetries are the only ones within which both the four-fold degeneracy ('unusual' case) appears for some levels and the two-fold degeneracy ('usual' case) appears for some other levels. This should be compared to the habitual two-fold (Kramers) degeneracy associated with *all* the levels known in all other deformed nuclei as e.g. in the case of the quadrupole deformation, see e.g., Ref. [3]. In fact, the symmetry-implied large shell gaps occur at some specific nucleon numbers and they can be comparable to the spherical shell-gaps. The tetrahedral magic numbers, N_t and Z_t,

for the neutrons and protons, respectively, are [4]: N_t or Z_t = 16, 20, 32, 40, 56, 68–70, 90–94, 112, and 136/142.

The possibility that tetrahedral symmetry is present in atomic nuclei has been discussed as early as in 1970'ies for ^{16}O in relation to the hypothetical four alpha-cluster structure [5–8]. Calculations employing the microscopic-macroscopic method [9], or the Skyrme Hartree-Fock (HFB) method [10–12] suggested that, in heavier nuclei, the tetrahedral shapes may appear in low-lying excited-, or even in the ground-states for specific nucleon numbers; see e.g. Refs. [13–16] for more recent works. It is, therefore, both timely and interesting to employ the well established methods of the theory of nuclear structure in an attempt of examining the leading features of the excitation spectra of collective motion associated with of the tetrahedral shape.

In this article we focus on certain properties of nuclear rotational bands in tetrahedral-deformed nuclei using advanced microscopic techniques which employ the angular-momentum and particle-number projection methods. Although the methods of performing the projections are straightforward and well-known [2, 17], their numerical realisation is a non-trivial task, especially for the non-axially symmetric and non-time-reversal invariant systems described using the cranking approximation (see e.g. Refs. [18, 19]). We have developed an efficient method to perform the projection from general and realistic mean-field wave functions calculated with large number of basis states [20]. Characteristic features of our method which have an important impact on an increased efficiency in the numerical realisation of the algorithm can be summarised as follows: (a) An efficient truncation scheme using the information about the occupation probabilities in the canonical basis; (b) The full use of the Thouless amplitude with respect to a Slater determinant state in place of the generalised Bogoliubov amplitudes; (c) Avoiding the sign problem for the norm overlap in terms of the Pfaffians [21] with using the Thouless amplitude.

The tetrahedral-symmetry nuclear-states have not been so far identified in nature. In order to facilitate the associated experimental research program in the case of a possible discovery of a new quantum phenomenon, one needs to establish first of all the global and leading characteristic properties of the tetrahedrally-symmetric nuclei. The main focus of the present article is to test the projection techniques associated with the mean-field methods, as far as the characteristic features of the energy spectra are concerned rather

than trying to be as realistic as possible in terms of the energy scale predictions. Another aspect is to test the projection techniques necessary to calculate the electromagnetic transition probabilities within the nuclear-mean field theory. Such transition probabilities and/or their branching ratios can be used as characteristic signs of the symmetries and will become a necessary tool for establishing such symmetries in nature. The related research program is in progress and results will be published elsewhere.

In the next Section, Sec. II, the principal mathematical expressions of the method are briefly recapitulated; the details can be found in Ref. [20]. The results of calculation are presented and discussed in Sec. III. The final section, Sec. IV, is devoted to the summary and possible future perspectives.

II. METHOD OF CALCULATION

In what follows we assume that a nucleus is in a state corresponding to a tetrahedral-symmetry minimum, one possibly among other competing minima in the total energy landscape. Assuming purely static configurations, i.e., ignoring the collective effects such as the zero-point vibrations or any other form of, e.g., large-amplitude motion which may be particularly needed in the case of the flat energy landscapes, we will calculate the excitation pattern using the angular-momentum, parity, and particle-number projection techniques, the latter in relation to pairing, combined with the mean-field techniques.

Thus, the most general symmetry-conserving wave function is sought in the form

$$|\Psi^{I(\pm)}_{M\alpha}\rangle = \sum_K g^{I(\pm)}_{K,\alpha}\, \hat{P}^I_{MK} \hat{P}_\pm |\Phi\rangle, \tag{1}$$

where $\hat{P}^I_{MK}$ and $\hat{P}_\pm$ are the angular-momentum and parity projectors (see e.g. Ref. [2]). The mean-field state $|\Phi\rangle$ is taken in the form of the anti-symmetrised product (HFB type) wave-functions, which is specified in Sec. II A. The K-mixing coefficients, $g^{I(\pm)}_{K,\alpha}$, are obtained by solving the generalised eigen-value problem of the Hill-Wheeler equations

$$\sum_{K'} \mathcal{H}^{I(\pm)}_{KK'}\, g^{I(\pm)}_{K',\alpha} = E^{I(\pm)}_\alpha \sum_{K'} \mathcal{N}^{I(\pm)}_{KK'}\, g^{I(\pm)}_{K',\alpha}, \tag{2}$$

with the Hamiltonian and norm kernel matrices being defined as usual as:

$$\begin{pmatrix} \mathcal{H}^{I(\pm)}_{KK'} \\ \mathcal{N}^{I(\pm)}_{KK'} \end{pmatrix} = \langle\Phi| \begin{pmatrix} \hat{H} \\ 1 \end{pmatrix} \hat{P}^I_{KK'} \hat{P}_\pm |\Phi\rangle. \tag{3}$$

In the present approach we wish to go beyond the mean-field approximation without perturbing the tetrahedral symmetry of the problem. This can be done by introducing in Eq. (3) a two-body spherically-symmetric Hamiltonian $\hat{H}$, whose form will be discussed in Sec. II B.

The neutron and proton number projections require the number projectors ($\hat{P}^N$ and $\hat{P}^Z$), which are further included in Eqs. (1)−(3). However, we found that the effect of the number projections on the quantum spectra in the present work is small, see Sec. III B, and they are simply neglected in most cases after verifying that such a neglect is justified.

A. Mean-Field Model and Its Hamiltonian

It is often of interest to employ the consistency condition between the mean-field and the many-body Hamiltonians like, e.g., in the Skyrme-Hartree-Fock models, since it is believed that such a consistency offers a more realistic description of the many-body systems in question. In this article we wish to focus first of all on the nuclear excitation spectra in the presence of pure tetrahedral symmetry of the mean-field. In this context it is preferable to work with the model allowing to completely control the deformation and the underlying geometrical symmetry. For this purpose, a phenomenological deformed mean-field is more convenient.

We use the product-type states composed of the eigen-functions of the Woods-Saxon (WS) potential [22], for which the general deformed shape is parametrised with the help of the spherical-harmonic $\{Y_{\lambda\mu}\}$-basis:

$$R(\theta,\varphi) = R_0\, c_v(\{\alpha\})\left[1 + \sum_{\lambda\mu} \alpha^*_{\lambda\mu} Y_{\lambda\mu}(\theta,\varphi)\right], \tag{4}$$

where the coefficient $c_v(\{\alpha\})$ takes care of the volume-conservation condition. In the present application, the pure tetrahedral deformation is realised by requiring all deformation parameters $\alpha_{\lambda\mu} = 0$ except α_{32} (more precisely, α_{3+2} and α_{3-2}). In this particular case, the problem of the centre of mass does not arise since tetrahedral-symmetric uniform-distributions preserve the position of the centre of mass independently of the value of the tetrahedral deformation. The deformed WS single-particle Hamiltonian, $\hat{h}_{\rm def}$, is diagonalized in the spherical harmonic oscillator basis with the oscillator quantum numbers n and l satisfying the usual relations $n_x + n_y + n_z = 2n + l \leq N_{\rm max}$.

The HFB type product state is obtained by further including the monopole pairing field with the particle number constraint:

$$\hat{h}_{\rm pair} = -\sum_{\tau={\rm n,\,p}} \Delta_\tau \left(\hat{P}^\dagger_\tau + \hat{P}_\tau\right) - \sum_{\tau={\rm n,\,p}} \lambda_\tau \hat{N}_\tau. \tag{5}$$

The pairing gap Δ in the Hamiltonian above is either parametrised, cf. Sec. II C, or self-consistently calculated by using the HFB treatment assuming the seniority interaction for neutrons and protons,

$$\hat{H}_P = -\sum_{\tau={\rm n,\,p}} G_\tau\, \hat{P}^\dagger_\tau \hat{P}_\tau. \tag{6}$$

The simple-minded usage of this pairing interaction with large model space may lead to a divergence. We replace the monopole pairing operator, $\hat{P}^\dagger$, by the one with a cut-off function, $f_{\rm c}(\epsilon)$,

$$\hat{P}^\dagger = \sum_{i>0} d^\dagger_i d^\dagger_{\tilde{\imath}} \quad \rightarrow \quad \sum_{i>0} f_c(\epsilon_i)\, d^\dagger_i d^\dagger_{\tilde{\imath}}, \tag{7}$$

where the quantity ϵ_i and $d^\dagger_i$ are the eigen-energy of the deformed WS single-particle state and its creation operator, respectively, so that $\hat{h}_{\rm def} = \sum_i \epsilon_i d^\dagger_i d_i$, and $\tilde{\imath}$ refers to the time-reversal conjugate-state of i. The form of the cut-off function is chosen to be [23],

$$f_{\rm c}(\epsilon) = \frac{1}{2}\left[1 + {\rm erf}\left(\frac{\epsilon - \lambda + \Lambda_{\rm low}}{d_{\rm cut}}\right)\right]^{1/2} \left[1 + {\rm erf}\left(\frac{-\epsilon + \lambda + \Lambda_{\rm up}}{d_{\rm cut}}\right)\right]^{1/2}, \tag{8}$$

with the error function defined as usual by ${\rm erf}(x) = \dfrac{2}{\sqrt{\pi}} \displaystyle\int_0^x e^{-t^2} dt$. Following Ref. [23] the parameter values adopted here are: $\Lambda_{\rm up} = \Lambda_{\rm low} = 1.2\,\hbar\omega$ and $d_{\rm cut} = 0.2\,\hbar\omega$ with $\hbar\omega = 41/A^{1/3}$ MeV. The chemical potential λ in Eq. (8) is simply chosen as $(\epsilon_{i_0} + \epsilon_{i_0+1})/2$, where i_0 is the last occupied orbital in the case of no pairing. Such a treatment results in preserving typically $+$(25-to-35) and $-$(15-to-25) states around the Fermi level for Rare Earth nuclei depending somewhat on the deformation used.

In the present article we wish to account, even if in a model dependent way, for at least some microscopic mechanisms whose existence is known already. In particular we are interested in the rotational state wave functions for increasing angular momenta. It is known that an increase of the angular momentum causes an increasing effect of the Coriolis coupling, the latter resulting in a gradual increase in the rotation-induced K-mixing. Since the presence of angular momentum introduces an extra direction in space, on top of the original tetrahedral symmetry, the latter is gradually more and more

perturbed. Studying of tetrahedral symmetry of a microscopic many-body system under the condition of increasing spin is a matter of a compromise between the original mean-field symmetry-properties and the Coriolis perturbation. As long as the Coriolis effects can be considered small, one may talk about the tetrahedral symmetry in the system.

In the pure mean-field context the rotational motion has been studied in the past by simulating the Coriolis coupling effects with the so-called cranking term which is linear in angular momentum and which contains the Lagrange multiplier ω in the case of the one-dimensional rotation. More generally, in the case of three-dimensional rotation, as in the present case, a triplet of Lagrange multipliers $\{\omega_x, \omega_y, \omega_z\} \equiv \boldsymbol{\omega}$ is introduced. The notation can be shortened to $\boldsymbol{\omega} = \omega\, \boldsymbol{n}$, where the unit vector $\boldsymbol{n}$ points to the direction of the total spin. One can show further that the term $\boldsymbol{\omega}$ can be given an *interpretation* of the rotational frequency valid asymptotically for increasing spin and regular nuclear energy-vs.-spin dependence – where from the notation $\boldsymbol{\omega} \to \boldsymbol{\omega}_{\rm rot}$.

To take into account the tetrahedral symmetry mean-field, here through $\hat{h}_{\rm def}$, the pairing correlation through the term $\hat{h}_{\rm pair}$, which does not impact the symmetry considerations, and a gradual effect of the Coriolis mechanism through the ($|K| = 1$)-mixing term, $\hat{h}_{|K|=1}$, we finally introduce the mean-field Hamiltonian

$$\hat{h}'_{\rm mf} = \hat{h}_{\rm def} + \hat{h}_{\rm pair} + \hat{h}_{|K|=1}, \qquad \hat{h}_{|K|=1} \equiv -\omega_{\rm rot}\, \boldsymbol{n} \cdot \hat{\boldsymbol{J}}. \tag{9}$$

As it turns out the third term in the above equation with a small $\boldsymbol{\omega}_{\rm rot}$, typically of the order of $\hbar\omega_{\rm rot} = 0.010$ MeV, is sufficient to break the time-reversal invariance and to introduce the ($|\Delta K| = 1$) K-mixing in the wave function, which is important to obtain more reliably the moment of inertia [20] within the Hill-Wheeler system of equations for the states not far from the ground-state. It has been tested, cf. Fig. 7 in Ref. [20], that the resulting spectra do not depend very much on the particular choice of values of $\hbar\omega_{\rm rot}$, as long as the spin values involved are not too high. Since in this paper we are interest in the spins of up to a dozen of $\hbar$, the particular value of this coefficient does not play any essential role and we keep the above value without modification for the present purpose.

Let us emphasise that the present use of the third term in Eq. (9), as compared to its role in the standard cranking model, is different. Whereas in the cranking-model approach in numerous articles on the high spin physics, $\omega_{\rm rot}$ plays either the role of the Lagrange multiplier adjusted to each new spin value and thus, on the average, increasing with spin,

or, alternatively, is currently being used as an independent cranking variable in function of which observables such as e.g. single-nucleon Routhians are plotted – here it may be seen as a coupling constant in front of a certain phenomenological interaction term.

B. Two-Body Model Hamiltonian for Projection Calculations

As commented already earlier, we wish to go beyond the mean-field approximation to be able to take into account, at least partially, certain two-body correlations which have proven to be successful in a phenomenological description of not strongly-deformed nuclei. For this purpose, we employ the model Hamiltonian used in the Hill-Wheeler formalism, cf. Eqs. (1)−(3), with an auxiliary spherically-symmetric WS potential and separable, schematic two-body interactions as the ones employed in Ref. [20]. The two-body Hamiltonian of this form does not perturb the tetrahedral symmetry, whereas at the same time allows for including a richer structure of the nucleon-nucleon interactions.

More specifically, we define

$$\hat{H} = \hat{h}_0 + \hat{H}_F + \hat{H}_G, \tag{10}$$

where $\hat{h}_0$ is a one-body Hamiltonian composed of the kinetic energy term and the spherical WS potential (with the Coulomb interaction for protons). The schematic particle-hole (F-type) interaction, $\hat{H}_F$, is chosen to be isoscalar and is defined by

$$\hat{H}_F = -\frac{1}{2}\,\chi \sum_{\lambda\geq 2} \sum_{\mu} : \hat{F}^{\dagger}_{\lambda\mu} \hat{F}_{\lambda\mu} :, \qquad \hat{F}_{\lambda\mu} = \sum_{\tau=\mathrm{n,\,p}} \hat{F}^{\tau}_{\lambda\mu}, \tag{11}$$

where : : denotes the normal ordering and $\tau = \mathrm{n}$, p distinguishes neutrons and protons. Furthermore, the spatial representation of the above particle-hole type operator, $\hat{F}^{\tau}_{\lambda\mu}$, is defined through the one-body field,

$$F^{\tau}_{\lambda\mu}(\boldsymbol{r}) = R^{\tau}_0 \,\frac{dV^{\tau}_c}{dr}\, Y_{\lambda\mu}(\theta,\phi), \tag{12}$$

with $V^{\tau}_c(r)$ and R^{τ}_0 being the central part of the WS potential and its radius, respectively. The so-called self-consistent value [1] of the force strength, χ, common to all multipolarities, is calculated by

$$\chi = (\kappa_n + \kappa_p)^{-1}, \qquad \kappa_\tau \equiv (R^{\tau}_0)^2 \int_0^{\infty} \rho^{\tau}_0(r) \frac{d}{dr}\left(r^2 \frac{dV^{\tau}_c(r)}{dr} \right) dr, \tag{13}$$

where $\rho_0^\tau(r)$ is the density of a hypothetical spherical ground state, which is calculated with the filling approximation for each nucleus based on the spherical WS single-particle state of $\hat{h}_0$. On the other hand, the pairing type (G-type) interaction, $\hat{H}_G$, acts only within like-particles, and is given by

$$\hat{H}_G = -\sum_{\tau=\mathrm{n,\,p}} \sum_{\lambda\geq 0} g_\lambda^\tau \sum_\mu \hat{G}^{\tau\dagger}_{\lambda\mu} \hat{G}^\tau_{\lambda\mu}, \qquad \hat{G}^{\tau\dagger}_{\lambda\mu} \equiv \frac{1}{2} \sum_{ij} \langle i|G^\tau_{\lambda\mu}|j\rangle c_i^\dagger c_{\bar{j}}^\dagger, \tag{14}$$

where the matrix elements of the pairing type operator, $\hat{G}^{\tau\dagger}_{\lambda\mu}$, are calculated with the help of the standard multipole form,

$$G_{\lambda\mu}(\boldsymbol{r}) = \left(\frac{r}{\bar{R}_0}\right)^\lambda \sqrt{\frac{4\pi}{2\lambda+1}}\, Y_{\lambda\mu}(\theta,\phi), \tag{15}$$

with $\bar{R}_0 = 1.2A^{1/3}$ fm.

The present formalism follows the main lines of Ref. [20] with a few modifications. Firstly, the extra one-body terms ($\hat{h}_1 = -\hat{h}_F - \hat{h}_G$ in §3.1 in [20]) are included in Ref. [20] in order to cancel out the one-body exchange contributions of the multipole interactions, $H_F + H_G$. It turns out that the effect of these terms on the resultant projected spectra is small, so that they are neglected for simplicity.

A slightly different deformed mean-field Hamiltonian has been used in Ref. [20], namely the one derived as the Hartree approximation to the interaction (11), in the form $\hat{h}_{\mathrm{def}} = \hat{h}_0 - \sum_{\lambda\mu} \alpha_{\lambda\mu} \hat{F}_{\lambda\mu}$, which, however, coincides with the central part of the present deformed WS potential only within the first order in the deformation parameters $\{\alpha_{\lambda\mu}\}$. We employ, in the present work, the general shape parameterisation based on the deformed radius in Eq. (4) with the volume-conservation condition properly taken into account. Moreover, the cut-off of the pairing model space is introduced directly in the operator $\hat{G}^{\tau\dagger}_{\lambda\mu}$ in Ref. [20]; then one has to use the spherical single-particle energy in the cut-off function (8) to keep the spherical invariance of the Hamiltonian. We found that it sometimes causes a problem that the results are rather sensitive to the choice of model space for the relatively small pairing model space like in the present case, $\Lambda_{\mathrm{u}} = \Lambda_{\mathrm{l}} = 1.2\,\hbar\omega$. In the present calculation, the cut-off of the pairing model space is taken into account in the step of deformed HFB calculation in Eqs. (9)−(7) based on the deformed WS single-particle state. Therefore, the cut-off function is not included explicitly in the pairing operator $\hat{G}^{\tau\dagger}_{\lambda\mu}$ anymore.

C. Choice of Parameters

The deformed mean-field single-particle states are calculated in the present work using the Woods-Saxon potential. An often used parameterisation introduced over thirty years back is referred to as 'universal' (cf. Refs. [24–28]). We employ, in this work, a new improved "universal compact" set, whose parameters are listed in Table I, see Ref. [22] for notations.

TABLE I: The parameters of the Woods-Saxon potential used in this work. Symbols ν and π refer to neutrons and protons, respectively.

	V_{0c} [MeV]	κ_c	r_{0c} [fm]	a_c [fm]	λ	V_{0so} [MeV]	κ_{so}	r_{0so} [fm]	a_{so} [fm]
ν	−52.0	0.650	1.26	0.64	28.0	49.6	0	0.870	0.70
π	−53.0	0.526	1.27	0.71	23.0	49.6	0	0.888	0.86

As for the maximum number of the harmonic oscillator shells to be used in the calculation, we employ $N_{\max} = 20$, which is a safe margin to accurately calculate the single-particle wave functions of the bound-states in the Woods-Saxon potential, and at the same time guarantees the convergence of the result of projection calculations [20].

The ground state deformation is determined for each nucleus by the axially symmetric WS-Strutinsky calculation of Ref. [23], where an algorithm allowing for the treatment of nuclei with weakly bound nucleons has been implemented. In the present realisation we calculate the strength of the seniority force, G, so as to reproduce the even-odd mass differences with the calculated deformation. More precisely, for the calculated equilibrium (ground state) deformations, α_{20} and α_{40}, we adjust the G-values in such a way that the calculated pairing gap, $\Delta_\tau = G_\tau \langle \hat{P}^\dagger_\tau \rangle$ (τ=n, p), agrees with the even-odd mass difference. Once the parameters G are fixed in this way, the usual BCS or the HFB equations (in the case of the cranking Hamiltonian) are solved self-consistently at any given deformation.

As for the spherically-symmetric Hamiltonian used for the projection calculation, the self-consistent value χ for the F-type interaction in Eq. (13) is used without any modifications. We include the $\lambda = 2, 3, 4$ components for the F-type interaction in Eq. (11), because the α_{20} and α_{40} deformations are taken into account for the ground state within the Strutinsky method and the tetrahedral shape is described by the α_{32} deformation. As

for the G-type interaction, the monopole pairing is known to be essential. It has been recognised that the quadrupole pairing interaction is also important especially to describe the rotational motion [1]. Therefore we include the $\lambda = 0, 2$ components for the G-type interactions in Eq. (14). The strength of the monopole pairing is determined again to reproduce the pairing gap, i.e., $\Delta_\tau = g_0^\tau \langle \hat{G}_{00}^{\tau\dagger} \rangle$ (τ=n, p), for the ground state wave function. As for the strength of the quadrupole pairing we assume $g_2^\tau / g_0^\tau = 13.6$, which is determined to approximately reproduce the moment of inertia of the ground state bands in the previous calculation [20]. Note that the values of G_τ and g_0^τ are slightly different, because the monopole pairing operator $\hat{P}_\tau^\dagger$ and the associated strength, G_τ, are defined with respect to the deformed WS basis, while the corresponding operator $\hat{G}_{00}^{\tau\dagger}$ and its strength, g_0^τ, are defined with respect to the spherical WS basis.

The model space truncation in the projection calculation is controlled by the small parameter ϵ defined through the requirement, that the orbitals which in canonical representation have occupation probabilities $v_i^2 > \epsilon$ are included, and, similarly, the core orbitals with $1 - v_i^2 < \epsilon$. We have chosen $\epsilon = 10^{-6}$ in the present calculation, with which it is confirmed that the resultant projected energies are stable within in 1 keV, which corresponds to six digits of accuracy for absolute energy of the present Hamiltonian in Eq. (10). As for the calculation of the Hill-Wheeler Eq. (1), the states that have smaller norm eigen-values than 10^{-10} are excluded.

III. RESULTS OF THE CALCULATIONS

According to the calculations in Refs. [4, 9], the tetrahedral magic numbers are N_t or Z_t = 16, 20, 32, 40, 56 – 68, 70, 90 – 94, 112, and 136/142, and are the same for the neutrons and protons. Calculations which followed, Refs. [29], figure 3, and [30], using the universal Woods-Saxon mean-field Hamiltonian, suggested that, in particular, $^{80}_{40}\mathrm{Zr}_{40}$ and $^{96}_{40}\mathrm{Zr}_{56}$ are tetrahedrally-symmetric in their ground-states, whereas tetrahedral minima lie about 1 MeV above the ground-state in $^{110}_{40}\mathrm{Zr}_{70}$. Skyrme Hartree-Fock calculations for the latter nucleus predict the possibility of the tetrahedral minima being the lowest – depending strongly on the choice of the model parameters [13]. More recently, we have reported on the calculations of the tetrahedral spectra in ^{108,110}Zr, in Ref. [31]. The predicted shape

coexistence in the Zirconium region which includes tetrahedral symmetry minima may give rise to, among others, the presence of isomeric states. Quite recently the experiment have been performed for unstable nucleus ^{108}Zr and the results are compatible with the existence of an isomeric state [32] whose nature is being debated.

A. Remarks about Symmetry Properties and Quantum Rotors

One of our goals is to determine whether the microscopic calculations which combine various advanced techniques of the nuclear quantum mechanics reproduce the excitation pattern predicted by group-representation theory. Because all of the two-fold and four-fold degenerate single-particle states are occupied with equal probabilities for the doubly-closed shell tetrahedral configurations, the totally symmetric, so-called *tensor* A_1 irreducible representation of the tetrahedral point-group T_d (as opposed to the *spinor* irreducible representations characterising the symmetry properties of the single-nucleonic wave-functions within the tetrahedral double-point group T_d^D, cf. also Table VIII in Appendix) can be expected as the resulting symmetry of the full system in its lowest rotational band. The situation remains the same if the seniority-type pairing interaction is effective for fully paired even-even nuclei.

An ideal tetrahedral (T_d-symmetric) classical rotor is often referred to as 'spherical', because its moment of inertia tensor is diagonal with all elements strictly equal. In the case of a quantum rotor, the notion of the inertia tensor cannot be strictly-speaking defined since the only quantum observables directly associated with rotational motion of such an object are the energy and angular momentum. The specific spectral properties of *quantum rotors with point-group symmetries* have been actively studied in relation to the TetraNuc Collaboration activities in recent years. For instance, examples of the octupole-symmetric quantum-rotor spectra have been presented in Ref. [33]; similar examples for specifically tetrahedral-symmetric quantum rotors can be found in Ref. [34] whereas the underlying tensor formalism and the general form of the reduced matrix elements are presented in Ref. [35]. Observe that in contrast to the 'usual' quantum rotor Hamiltonians discussed in the literature, which are quadratic forms of the angular momentum operators, the tetrahedral (or other octupole-symmetric) rotor Hamiltonians are specific third-order

forms expressed in terms of the operators $\{\hat{I}_x, \hat{I}_y, \hat{I}_z\}$ (equivalently of $\{\hat{I}_{-1}, \hat{I}_0, \hat{I}_{+1}\}$ using spherical tensor representation). Furthermore, relations between the energy spectra of the quantum rotors and the associated properties of classical rotors have been discussed in Ref. [36].

It can be shown that the spectra of tetrahedral-symmetric structure-less quantum rotor are composed of the $(2I+1)$-degenerate states for each given spin I, cf. Ref. [34]. In this sense the spherical-symmetry of the classical tetrahedral rotor mentioned above and the symmetry of the tetrahedral quantum rotor can be seen as analogous. According to group-theory considerations, each of the $(2I+1)$-degenerate states of the T_d-symmetric structure-less rotor of any given I belongs to a certain specific irreducible representation of the group in question. Among five of those irreducible representations, the A_1 (scalar) representation contains states with the following characteristic set of spin-parity combinations [cf. Table VI in the Appendix (also e.g. Ref. [38, 39])]:

$$0^+,\, 3^-,\, 4^+,\, 6^+,\, 6^-,\, 7^-,\, 8^+,\, 9^+,\, 9^-,\, 10^+,\, 10^-,\, 11^-,\, 2\times 12^+,\, 12^-, \cdots . \qquad (16)$$

As it is discussed in more detail below, such characteristic spectra are indeed realised for the lowest energy band in the results of our microscopic calculation, cf. also Ref. [31].

It is worthwhile mentioning that there exist certain extra discrete symmetries for the tetrahedral shape nuclear mean-field configurations applying within the cranking model. They are referred to as *doublex* and *triplex* (as opposed to the 'usual' *simplex-symmetry* applying to the cranking model for the pear-shape symmetric nuclei). The corresponding quantum numbers are useful to further classify the characteristic spectra as discussed in Refs. [40, 41], but this issue goes beyond the scope of the present article.

In this work we report on the more extensive and detailed investigations for three doubly-closed tetrahedral-shell configurations in nuclei: ^{160}Yb ($Z = 70$ and $N = 90$), the already mentioned ^{110}Zr, as well as the heavier tetrahedral-symmetric nucleus in the Actinide region, ^{226}Th ($Z = 90$ and $N = 136$). The axially symmetric octupole (α_{30}) deformed states of the latter nucleus have also been studied in Ref. [20].

B. Tetrahedral-Symmetry in ^{160}Yb: Phonon-vs.-Rotation-Like Structures

Following the procedure of Sec. II C, we obtain the following parameters for the pairing force and residual interaction given in Table II, where the calculated deformation parameters for the ground state are also shown.

α_{20}	α_{40}	$\Delta_{\rm n}$ [MeV]	$\Delta_{\rm p}$ [MeV]	$G_{\rm n}$ [MeV]	$G_{\rm p}$ [MeV]	χ [MeV^{-1}]	$g_0^{\rm n}$ [MeV]	$g_0^{\rm p}$ [MeV]
0.194	0.031	1.265	1.370	0.1512	0.1732	2.643×10^{-4}	0.1468	0.1675

TABLE II: The calculated ground state deformation parameters (α_{20}, α_{40}), the 4-th order even-odd mass difference ($\Delta_{\rm n}$, $\Delta_{\rm p}$), and the force strength parameters determined based on them for $^{160}_{70}{\rm Yb}_{90}$. The value $g_2^\tau/g_0^\tau = 13.6$ is taken for the ratio of the quadrupole and monopole pairing.

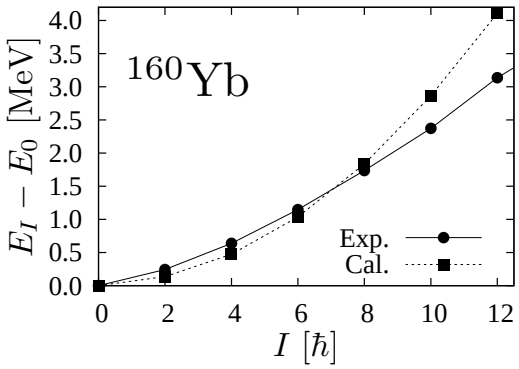

FIG. 1: Comparison of the experimental and the calculated rotational spectra in ^{160}Yb.

Let us begin by presenting the results of our projection calculations for the ground state band in ^{160}Yb; the corresponding results are shown in Fig. 1, where comparison with the experimental data can also be found. In this calculation, we use the HFB type wave function with a small Coriolis ($|\Delta K| = 1$)-coupling $\hbar\omega_{\rm rot} = 0.010$ MeV parameter, as discussed in Sec. II A. We choose the cranking axis as the y-axis, which is perpendicular to the symmetry axis (z-axis). The agreement of the calculated spectra with the experimental data is acceptable but discrepancies as compared to the experiment increase with spin. In particular, the observed moment of inertia increases as a function of spin, but the calculated moment of inertia is fairly constant. This trend was already found for other nuclei in Ref. [20] and may partly reflect the fact that in contrast to the cranking model,

within which the pairing correlations systematically decrease with cranking frequency and thus increase the moment of inertia, in the present model with projection from one mean-field state the mentioned mechanism does not exist. In the present calculation of the ground state the axial symmetry is broken only by a small ($|\Delta K| = 1$)-mixing term, and the mixing effect of the K quantum number in the Hill-Wheeler Eq. (2) remains small. Since this particular aspect is of secondary importance of the present project we accepted the disagreement in question as remaining under control but without consequences for the main conclusions. Doing so we may profit from a technical advantage: It is sufficient to use relatively small numbers of points for Gauss quadratures with respect to the Euler angles when performing the angular-momentum projection calculation, e.g., $N_\alpha = N_\gamma = 16$ and $N_\beta = 50$.

We proceed to examining the tetrahedral nuclear configuration and related rotational states. The simplest way to construct the tetrahedral shape in the surface parameterisation in Eq. (4) is to set $\alpha_{32} = \alpha^*_{32} = \alpha_{3-2}$ as the only non-zero deformation parameters. In the coordinate system chosen the upper ($z > 0$) and lower ($z < 0$) sides of the tetrahedron are parallel to the y- and x- axes, respectively, and the z-axis is along the line that connects the middle points of these two facing sides. Again, we have chosen the y-axis for cranking with a small frequency $\hbar\omega_{\rm rot} = 0.01$ MeV. Obviously, in this case the axial symmetry is strongly broken depending on α_{32} and thus higher order quadratures in the projection calculations are necessary. We take $N_\alpha = N_\gamma = N_\beta = 64$ for $\alpha_{32} = 0.1 - 0.2$, $N_\alpha = N_\gamma = N_\beta = 84$ for $\alpha_{32} = 0.25 - 0.30$, and $N_\alpha = N_\gamma = N_\beta = 104$ for $\alpha_{32} = 0.35 - 0.40$ for the calculation in this nucleus.

In Figure 2 we illustrate the result of excitation energies of the projected eigen-states, cf. Eq. (1), whose norm is not very small, i.e. not less than 10^{-5} of that of the ground state. They compose the lowest-energy sequence, and calculated for the pure tetrahedrally deformed configuration with deformations $\alpha_{32} = 0.05$, 0.10 and 0.20. As it is seen from the figure, only the specific spin-parity combinations appear, cf. Eq. (16), for all deformations. This pattern is characteristic for the tetrahedral symmetry and is quite different from the one of the usual quadrupole deformation. Indeed, the spectrum is composed of states characterised by 0^+, 3^-, 4^+, $6^\pm$, ...; the states with $I = 1$, 2 and 5 are missing in the figure since their norms are too small and/or they lie much higher in energy as compared

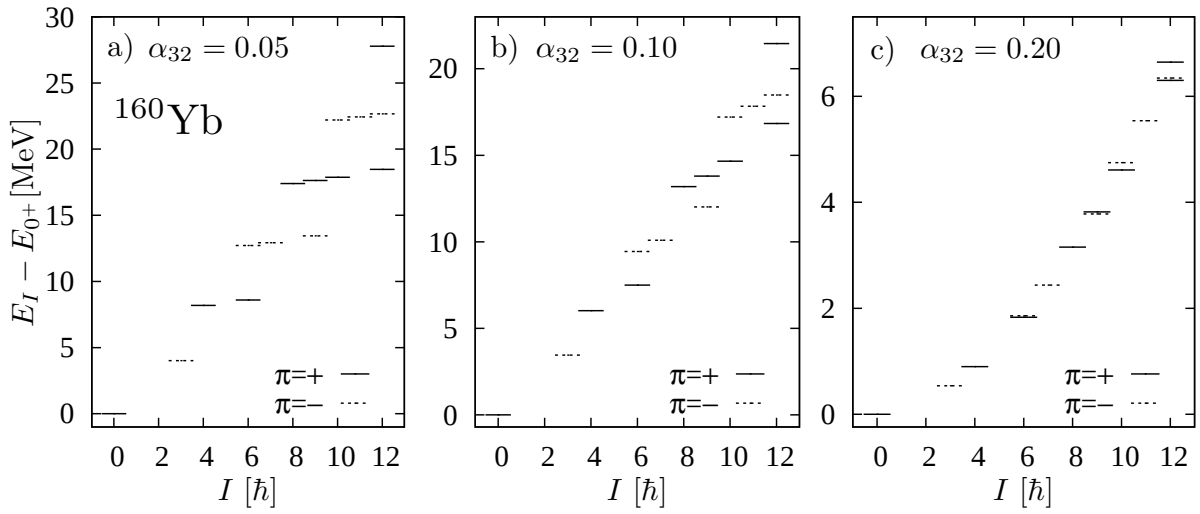

FIG. 2: Examples of calculated spectra of tetrahedral states belonging to the lowest energy part in the spectrum in ^{160}Yb with $\alpha_{32} = 0.05$ (left), $\alpha_{32} = 0.10$ (middle) and $\alpha_{32} = 0.20$ (right), testing the dependence of the excitation energies on the tetrahedral deformation [cf. also Eq. (16)]. The positive (negative) parity states are denoted by the solid (dotted) lines. Note the difference of ordinate-scales between the left and right panels.

to the discussed lowest-energy sequence.

A very small tetrahedral deformation of $\alpha_{32} = 0.05$ corresponds to nearly spherical form. The existence of collective excitations in spherically symmetric nuclei has long been recognised in terms of the vibrational modes, which results in an equidistant spectrum composed of multiplet of states, within the simplest harmonic representation, in terms of the vibration-quanta: The phonons, see e.g. Sect. (6.3.2) in Ref. [37].

The spectrum with smallest deformation $\alpha_{32} = 0.05$ in Fig. 2 is more vibrational-like, while that with $\alpha_{32} = 0.20$ is approaching to the rotational-like spectrum; the one with $\alpha_{32} = 0.10$ is in-between. In fact, $(4^+, 6^+)$, $(6^-, 7^-, 9,^-)$, $(8^+, 9^+, 10^+, 12^+)$ ... states in Fig. 2 a) having the same parity can be grouped together, and would be interpreted as slightly perturbed two-phonon, three-phonon, four-phonon ... multiplet structures, respectively, of an elementary mode of the 3^- vibrational excitation. Moreover, the excitation energies of 3^-, 6^+, 9^-, 12_1^+ form a rather linear dependence as a function of spin; the dependence resembles the pattern expected for the multi-phonon excitation. Note,

however, that only the specific spin states among the multi-phonon multiplets appear, which is a consequence of the tetrahedral symmetry. In contrast in Fig. 2 c), the states with the same spin value are nearly degenerate, which is a specific feature of the ideal rotor, and, at the same time, approximately follow the quadratic energy-vs.-spin relation, $E(I) \propto I(I+1)$.

Let us emphasise, that both the parity and the angular-momentum projections were essential for obtaining the tetrahedral-symmetry pattern predicted by the group theory. This symmetry pattern seems rather typical for the present model Hamiltonian: We obtain similar pattern also for other nuclei, e.g., ^{110,108}Zr [31] and ^{226}Th below. In the present work, we concentrate on the lowest energy sequence and we do not enter the discussion of the group theory aspects. Instead let us only mention that representations other than A_1 must be expected for excited bands; also – one may expect, that the symmetry in the case of the non-doubly-closed shell nuclei could be manifested less strongly.

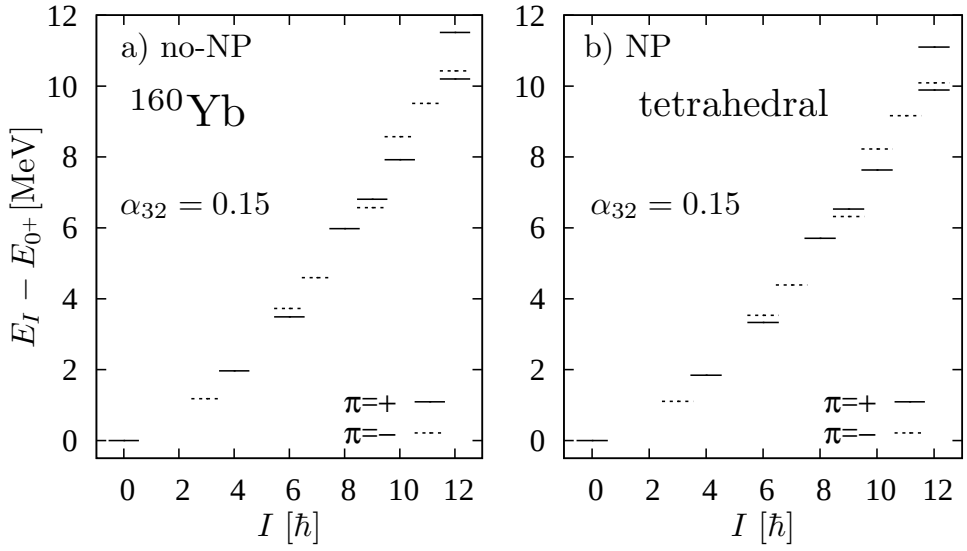

FIG. 3: Comparison of the spectra of tetrahedral states with (right) and without (left) the number projection (NP), which are shown in the same way as in Fig. 2 but with $\alpha_{32} = 0.15$.

In Figure 3 we compare the results of tetrahedral spectra with and without the particle-number projection (NP) related to pairing formalism. Although the moments of inertia (the slopes) are slightly different, the characteristic properties of the spectra are exactly the same in the two calculations. We conclude that the effect of the particle number

projection is small and we do not apply it in the rest of the article.

C. Transition to Ideal Rotor and Moments of Inertia in ^{160}Yb

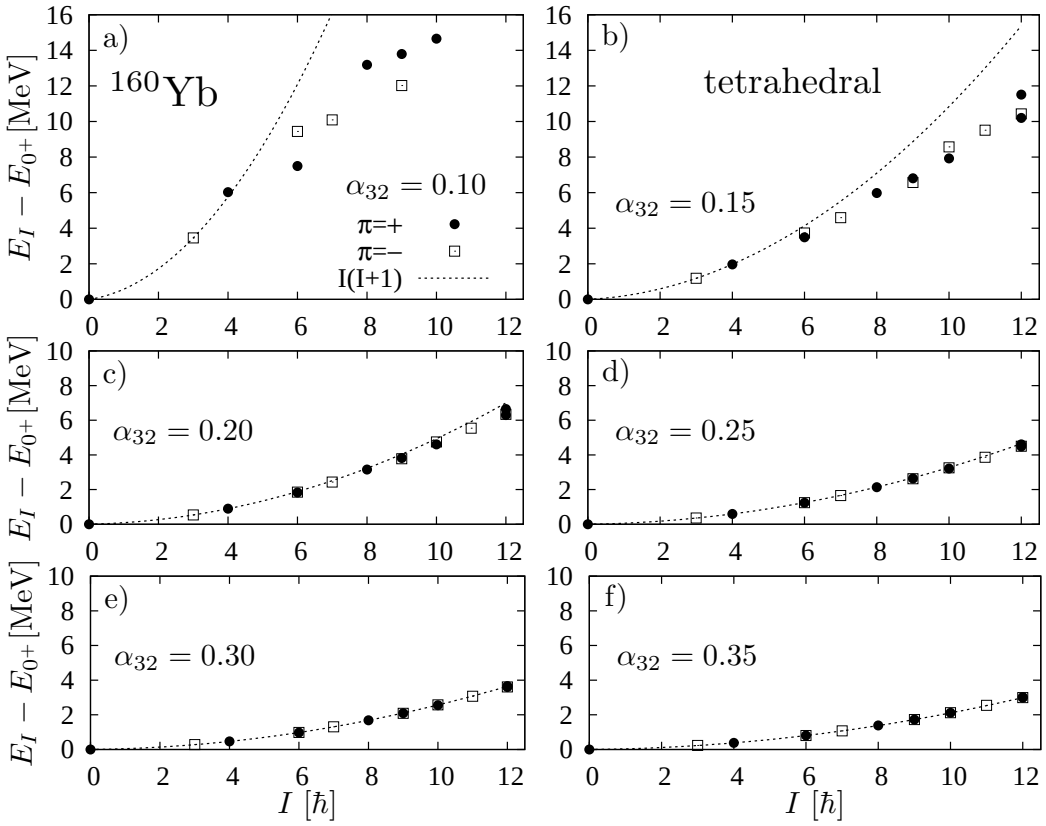

FIG. 4: Calculated spectra of tetrahedral states in ^{160}Yb with $\alpha_{32} = 0.10$, 0.15, 0.20, 0.25, 0.30, and 0.35, respectively, for a), b), c), d), e), and f). The dotted line in each panel denotes an ideal $I(I+1)$ sequence going through the first excited 3^- state. Note that almost exact degeneracies for $I = (6^+, 6^-), (9^+, 9^-), (10^+, 10^-), (2{\times}12^+, 12^-)$ states are obtained for $\alpha_{32} \geq 0.25$ demonstrating the nearly perfect rotor character of the rotational excitation of the system.

The fact that the tensor of inertia of an ideal classical tetrahedral rotor is diagonal with all components equal ('spherical rotor') suggests that the tilting direction of the cranking axis in Eq. (9) may not affect the tetrahedral spectra, at least to the extent in which the Coriolis alignment effects can be neglected, i.e., for not too high spins. In order to test this conjuncture, we investigated the projected spectra from the cranked mean-field state

with the different tilted cranking axes. We have varied the cranking axis in our coordinate system, i.e. the vector $\boldsymbol{n}$ in the term, $\hat{h}_{|K|=1} \equiv -\omega_{\rm rot}\, \boldsymbol{n} \cdot \hat{\boldsymbol{J}}$, in Eq. (9) is changed by

$$\boldsymbol{n} = (\sin\theta \sin\varphi, \cos\theta, \sin\theta \cos\varphi), \qquad 0 \leq \theta \leq 90^\circ, \quad 0 \leq \varphi \leq 45^\circ. \tag{17}$$

We found that the differences of the resulting spectra for the lowest energy sequence are negligible within the accuracy of our calculation; i.e. the nature of 'spherical rotor' is numerically confirmed. More generally, the projected spectra for the tetrahedral symmetric nuclei do not depend on the $|\Delta K| = 1$ coupling term, both the strength $\omega_{\rm rot}$ and and the direction $\boldsymbol{n}$ of the tilted cranking axis, as long as $\omega_{\rm rot}$ is small.

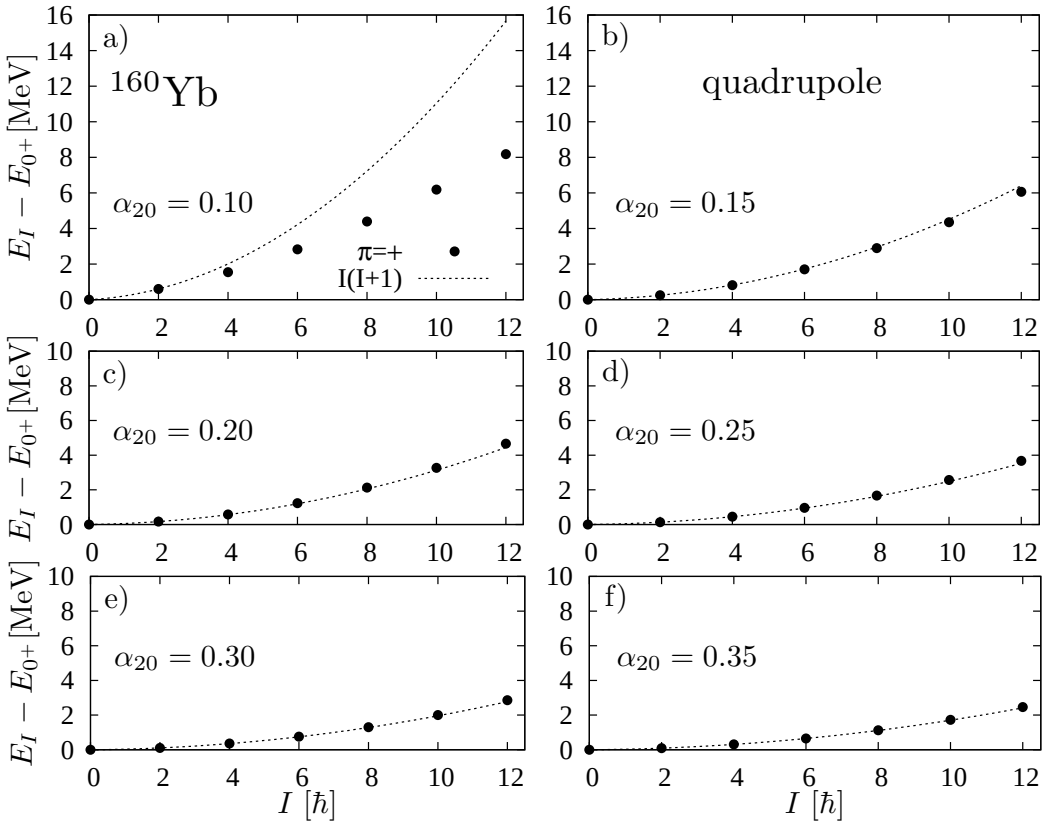

FIG. 5: Calculated spectra of quadrupole deformed states in ^{160}Yb with $\alpha_{20} = 0.10$, 0.15, 0.20, 0.25, 0.30, and 0.35, respectively, for a), b), c), d), e), and f). The dotted lines in each panel denote the ideal $I(I+1)$ spectra going through the first excited 2^+ state.

In Figure 4 we show the calculated excitation energies for selected values of the tetrahedral deformation. The ideal rotor spectra with the energies proportional to $I(I+1)$

and containing the calculated first excited 3^- states are also shown by the dotted lines. This figure clearly shows that the spectra exhibit the gradual transition from linear to parabolic spin dependence with increasing the tetrahedral deformation: The almost ideal rotor spectrum is realised for $\alpha_{32} \gtrsim 0.25$.

Now we compare the tetrahedrally-symmetric spectra with those of the quadrupole deformation. In Figure 5 we show the results of calculated spectra obtained by the angular-momentum projection from the pure quadruple deformed states, where all the deformation parameters are set to zero except α_{20} (no parity projection is required in this case). The projection calculation tends to give good rotational spectra, but the result with small deformation, $\alpha_{20} = 0.10$, considerably deviates from the one for the pure rotor spectra. Thus the gradual transition from the linear to parabolic energy-vs.-spin dependence is seen also for the calculation of the quadrupole deformation.

Although the moment of inertia is *not* any quantum-mechanical observable, certain quasi-classical analogies often found in the literature allow to define and estimate the corresponding values. Here we define this parameter, $\mathcal{J}$, through

$$E(I) - E(0) = \frac{I(I+1)}{2\mathcal{J}}. \tag{18}$$

It is well-known that the moments of inertia of observed rotational band near the ground state are about (or even smaller than) half of the classical rigid-body value. This large reduction is supposed to be due to the pairing correlations [1, 42]. In fact, the moments of inertia extracted from the high-spin states, where the pairing correlations are believed to be quenched, are known to be close to the rigid-body value, although some deviations attributed shell effects exists, see e.g. Ref. [43]. Therefore, it is instructive to investigate the moment of inertia in the case of the tetrahedral rotor. In Figure 6 the moments of inertia calculated from Eq. (18) are plotted as functions of the tetrahedral (left) and the quadrupole (right) deformations, where they are estimated from the calculated 3^- and 2^+ excitation energies, respectively. The results with neglecting the pairing correlation and the rigid-body value are also included. An irregular behaviour for the unpaired ($\Delta = 0$) moments of inertia, i.e., at $\alpha_{20} \approx 0.20 - 0.25$, is due to the fact that the level crossings near the Fermi surface occur. In order to illustrate the possible correlation between the moments of inertia and the intensity of pairing correlations measured with the help of the pairing gaps, the calculated pairing gaps at corresponding deformations are shown in

Fig. 7.

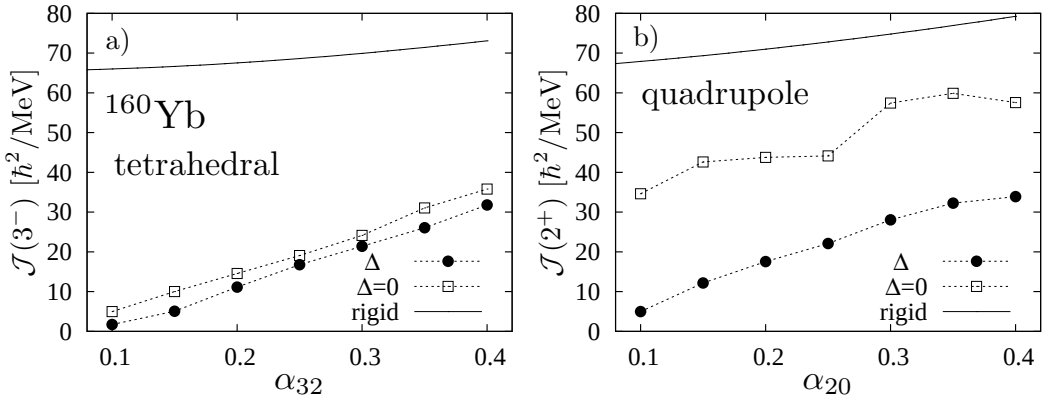

FIG. 6: Moment of inertia estimated from the calculated spectra for the pure tetrahedral states (left) and the pure quadrupole states (right) as functions of the deformation parameters in ^{160}Yb. The energy of the first excited 3^- (2^+) is used for estimation of the former (latter). The results with the pairing correlations artificially set to zero are also included. The classical rigid-body moments of inertia in function of the deformation parameters are shown as solid lines.

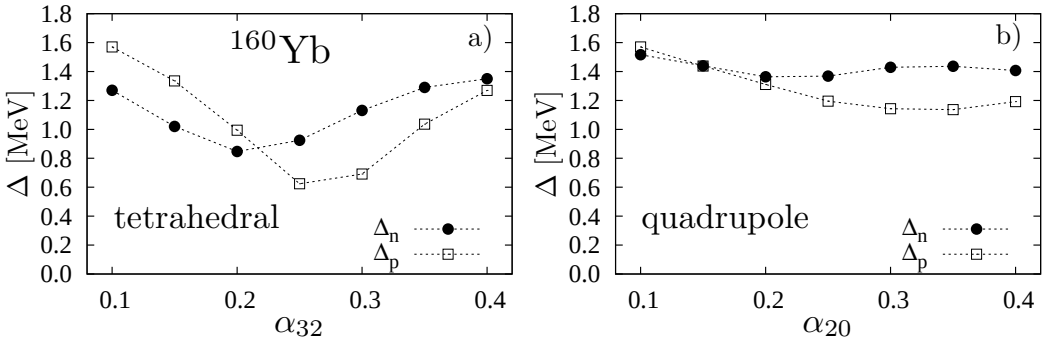

FIG. 7: The self-consistent neutron and proton pairing gaps for the tetrahedral states (left) and the quadrupole states (right) as functions of the respective deformation parameters in ^{160}Yb.

As it becomes clear from Fig. 6, the moment of inertia increases rapidly with increasing deformation for both the tetrahedral and quadrupole shapes, indicating that the picture of the good rotor emerges for larger deformation. Observe that the values of the moments of inertia at the two considered shape configurations are rather similar when the pairing correlations are included, and are both much smaller than the rigid-body values even at the largest value of the deformation parameters. If the pairing correlations are set to

zero, the calculated moment of inertia for the quadrupole shape becomes much larger and approaches to the rigid-body value as it is observed from the high-spin limit. However, the effect of pairing correlation on the inertia for the tetrahedral shape is rather small, even though the pairing gap takes more or less the same values as in the case of the quadrupole shape. The reason why the moment of inertia is small and is affected very weakly by the pairing correlation may be because the chosen nucleus in this case is the tetrahedral doubly-closed shell nucleus. The shell gap is $\sim 1.5-2$ MeV and is larger than the pairing gap, which is in contrast to the case of quadrupole deformation, where the mean single-particle level spacing is much smaller than the pairing gap.

D. Tetrahedral spectra in ^{110}Zr

The nuclear potential energy surfaces for the doubly-magic Zirconium nuclei have been studied in Ref. [29] and the corresponding illustrations obtained using the phenomenological approach with the Woods-Saxon mean-field Hamiltonian can be found in figure 3 of the above reference. The symmetry-oriented discussion of the corresponding shell-effects can be found in Ref. [44]. A discussion of the static-energy properties in a few nuclei in the vicinity of ^{110}Zr using Hartree-Fock approach can be found in Ref. [45], whereas the tetrahedral rotational properties, specifically for the nucleus ^{110}Zr, have been studied using the cranking-Skyrme-Hartree-Fock method in Ref. [46] and using the methods similar to that of the present article in Ref. [31].

In the present work the method of calculation is essentially the same as in [31], except that the different Woods-Saxon Hamiltonian parameter set is used. The mean-field parameters and the force strengths used in the present calculation are given in Table III. The calculated pairing gaps are used because the experimental even-odd mass differences are not available for this unstable nucleus. The numbers of nodes for the Gaussian quadratures are chosen to be $N_\alpha = N_\gamma = N_\beta = 64$ after verifying the stability conditions for the final result.

In Figure 8 we show the excitation energies for various deformations in function of angular momentum, obtained using the angular-momentum and parity projection techniques. The cranking axis is chosen to be the y-axis [$\theta = 0^\circ$ in Eqs. (9) and (17)]. As it is

α_{20}	α_{40}	$\Delta_{\rm n}$ [MeV]	$\Delta_{\rm p}$ [MeV]	$G_{\rm n}$ [MeV]	$G_{\rm p}$ [MeV]	χ [MeV^{-1}]	$g_0^{\rm n}$ [MeV]	$g_0^{\rm p}$ [MeV]
0.333	−0.026	1.129	1.113	0.1471	0.2698	4.785×10^{-4}	0.1407	0.2625

TABLE III: The calculated ground-state mean-field parameters (α_{20}, α_{40}, $\Delta_{\rm n}$, $\Delta_{\rm p}$), and the force strength parameters determined based on them for ${}^{110}_{40}{\rm Zr}_{70}$. The value $g_2^\tau/g_0^\tau = 13.6$ is taken for the ratio of the quadrupole and monopole pairing.

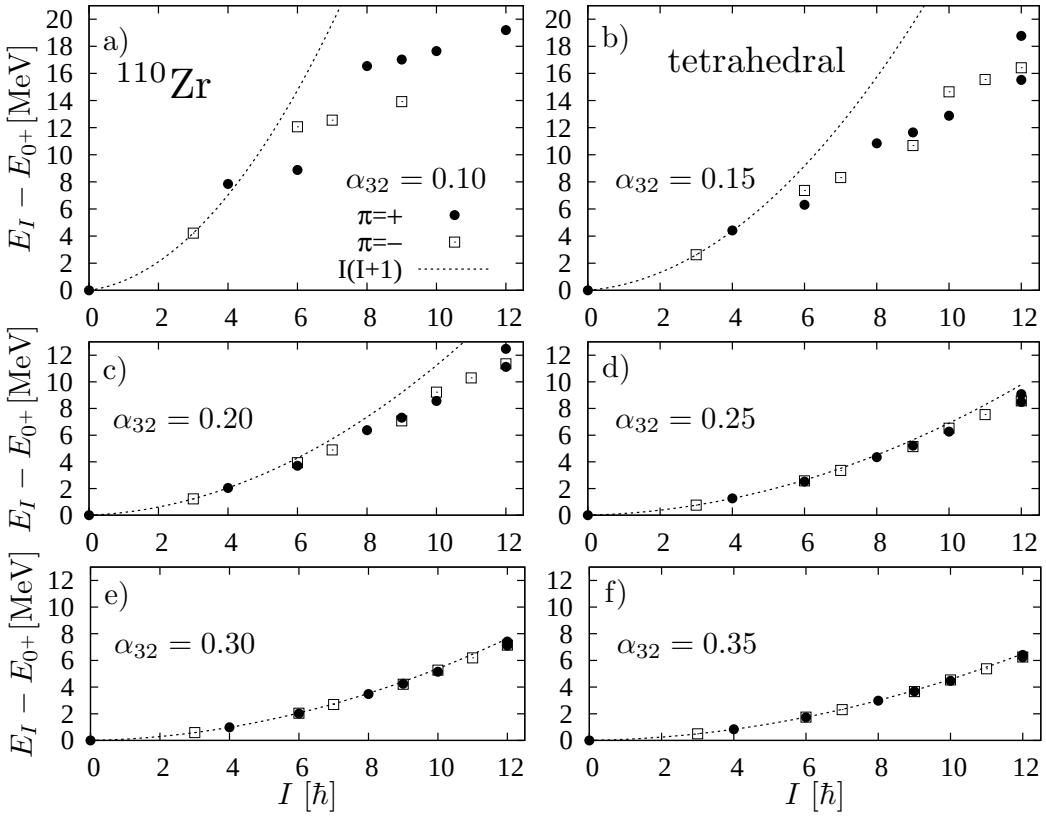

FIG. 8: Calculated spectra of tetrahedral states in ^{110}Zr with $\alpha_{32} = 0.10$, 0.15, 0.20, 0.25, 0.30, and 0.35, respectively, for a), b), c), d), e), and f). The figure is similar to that in Ref. [31] but only the lowest band is selected and the results for larger deformation are included. Note that almost exact degeneracies for $I = (6^+, 6^-), (9^+, 9^-), (10^+, 10^-), (2 \times 12^+, 12^-)$ states are obtained for $\alpha_{32} \geq 0.30$.

seen from the Figure, the over-all pattern of the excitation scheme resembles the one in ^{160}Yb. However, compared with the results for ^{160}Yb of Fig. 4, the transition to the ideal rotor occurs slower, i.e., it occurs at the larger deformation in the lighter system ^{110}Zr.

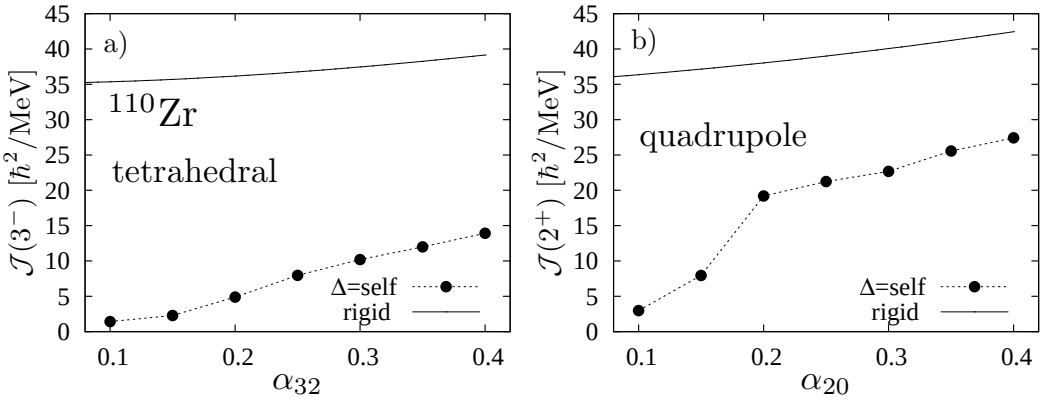

FIG. 9: Moment of inertia estimated from the calculated spectra for the pure tetrahedral states (left) and the pure quadrupole states (right) in ^{110}Zr. The energy of the first excited 3^- (2^+) is used for estimation of the former (latter). The rigid-body moment of inertia are shown as solid lines.

In particular, the energy-vs.-spin relation resembles a rigid rotation only for $\alpha_{32} \gtrsim 0.30$. Compared with the results in Ref. [31], those in the present work are very similar, indicating that the choice of the parameter set of the WS potentials very little affects the rotational properties of a tetrahedral symmetric nucleus – provided a realistic choice of parameters is used. We have checked the dependence of the projected energies on the tilting angle of the cranking axis also for the nucleus ^{110}Zr (cf. also figure 1 in Ref. [41]). Again, the result is found to stay the same, when the tilting angle is changed in the same way as in ^{160}Yb [cf. Eq. (17)].

In Fig. 9, the moments of inertia for the tetrahedral and quadrupole deformations are compared for the case of ^{110}Zr; only the results with pairing correlations are presented. As it is seen, the values of the moments of inertia for two types of deformations are slightly different; the ratio $\mathcal{J}(3^-)/\mathcal{J}_{\rm rigid}$ for the tetrahedral shape is considerably smaller than the ratio $\mathcal{J}(2^+)/\mathcal{J}_{\rm rigid}$ for the quadrupole shape. One of the reasons may be traced back to the somewhat larger shell gap at $Z = 40$ for the tetrahedral shape, so that the ratio $\mathcal{J}(3^-)/\mathcal{J}_{\rm rigid}$ in ^{110}Zr is smaller than that in ^{160}Yb. Furthermore, the pairing gaps for the quadrupole shape with $\alpha_{20} \geq 0.20$ are somewhat reduced in ^{110}Zr, which increases the quadrupole moment of inertia; those combined effects for the two types of shapes may make the difference of their behaviour in ^{110}Zr compared to the case of ^{160}Yb (and of

^{226}Th, see below).

E. Tetrahedral spectra in ^{226}Th

The calculation procedure for ^{226}Th is the same as that for ^{160}Yb and ^{110}Zr. The mean-field single-nucleon energies for this particular nucleus in function of tetrahedral deformation can be found in figure 4 of Ref. [47]. The parameters determined by the Woods-Saxon-Strutinsky calculation, and those of the force strengths are tabulated in Table IV. They are similar to the ones used in Ref. [20], where the α_{30} deformation was also taken into account. Slightly different values of the parameters as compared to those in Ref. [20] are mainly due to the fact that the different parameter set of the WS potential is employed. The computing time of the projection calculation increases dramatically with increase of the nucleon number as well as the numbers of the mesh points for Gaussian quadratures. We have carefully tuned the latter numbers for ^{226}Th to obtain the same accuracy as in the case of ^{160}Yb. Thus, we take $N_\alpha = N_\gamma = 64$ and $N_\beta = 74$ for $\alpha_{32} = 0.10 - 0.15$, $N_\alpha = N_\gamma = 104$ and $N_\beta = 84$ for $\alpha_{32} = 0.20$, $N_\alpha = N_\gamma = 124$ and $N_\beta = 104$ for $\alpha_{32} = 0.25 - 0.30$, and $N_\alpha = N_\gamma = N_\beta = 124$ for $\alpha_{32} = 0.35 - 0.40$.

α_{20}	α_{40}	$\Delta_{\rm n}$ [MeV]	$\Delta_{\rm p}$ [MeV]	$G_{\rm n}$ [MeV]	$G_{\rm p}$ [MeV]	χ [MeV^{-1}]	$g_0^{\rm n}$ [MeV]	$g_0^{\rm p}$ [MeV]
0.161	0.093	0.814	0.830	0.09772	0.1289	1.744×10^{-4}	0.09568	0.1267

TABLE IV: The calculated ground state deformation parameters (α_{20}, α_{40}), the 4-th order even-odd mass difference ($\Delta_{\rm n}$, $\Delta_{\rm p}$), and the force strength parameters determined based on them for $^{226}_{90}{\rm Th}_{136}$. The value $g_2^\tau/g_0^\tau = 13.6$ is taken for the ratio of the quadrupole and monopole pairing.

The result of our angular-momentum and parity projection calculations for various tetrahedral deformations are shown in Fig. 10. The characteristic features of the spectra resemble those of ^{160}Yb and ^{110}Zr. Again, the energy-vs.-spin dependence has approximately linear behaviour for smaller deformations, whereas it approaches a parabolic form at increasing deformation. Comparing the energy-vs.-spin dependence of these three nuclei, the transition from a linear to parabolic spin dependence occurs at smaller deformation in nuclei with larger mass number. More precisely, the energy-vs.-spin dependence becomes almost parabolic in the following proportions: at $\alpha_{32} \approx 0.15$ in ^{226}Th, at

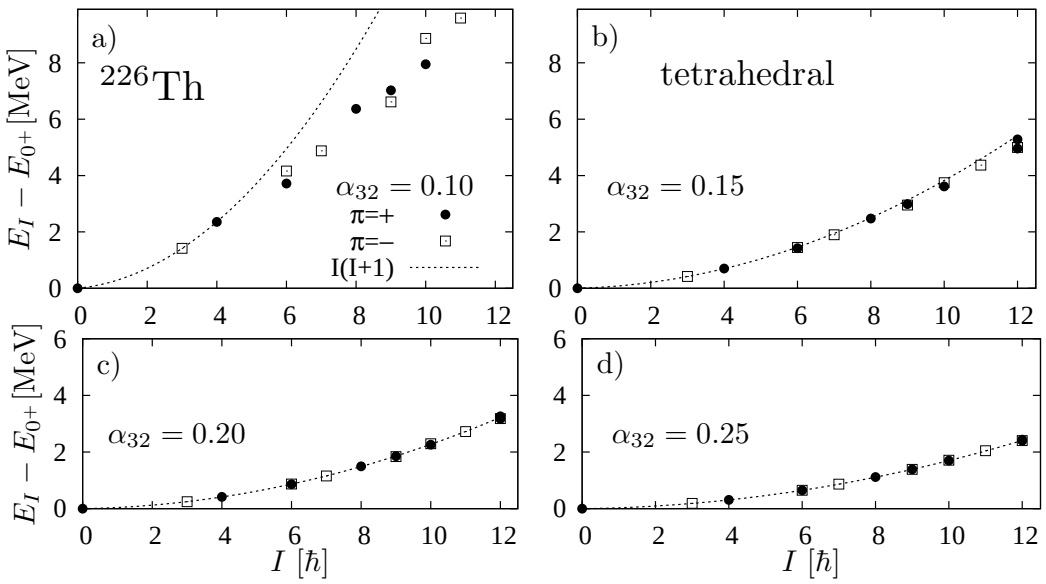

FIG. 10: Calculated spectra of tetrahedral-symmetry states in ^{226}Th with $\alpha_{32} = 0.10$, 0.15, 0.20, and 0.25 respectively, for a), b), c), and d). Note that almost exact degeneracies for $I = (6^+, 6^-), (9^+, 9^-), (10^+, 10^-), (2 \times 12^+, 12^-)$ states are obtained for $\alpha_{32} \geq 0.20$.

$\alpha_{32} \approx 0.20$ in ^{160}Yb, and at $\alpha_{32} \approx 0.25$ in ^{110}Zr. This is intuitively acceptable because the concept of the symmetry-breaking is more and more appropriate for heavier nuclear systems.

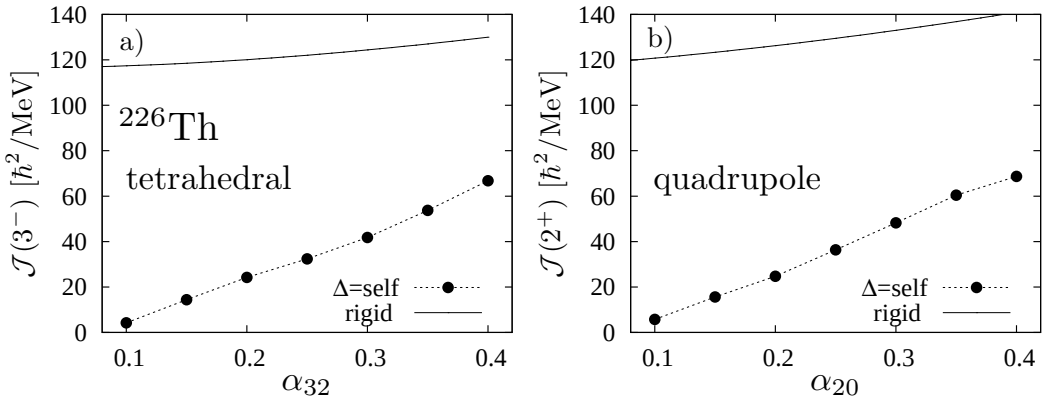

FIG. 11: Moments of inertia estimated from the calculated spectra for the pure tetrahedral states (left) and the pure quadrupole states (right) in ^{226}Th. The energy of the first excited 3^- (2^+) is used for estimation of the former (latter). The classical rigid-body moments of inertia are shown as solid lines.

The calculated moments of inertia as functions of quadrupole and tetrahedral deformation parameter are illustrated in Fig. 11, where only the result including the pairing correlation is shown. Again, the moments of inertia with the pairing correlation are considerably smaller than the rigid-body values and they increases with deformation. The values of moment of inertia are rather similar for the tetrahedral and quadrupole shapes in ^{226}Th as in the case of ^{160}Yb in Fig. 6.

IV. SUMMARY

We have studied the rotational nuclear properties for the pure tetrahedral deformation by the angular-momentum and parity projection method employing the realistic Woods-Saxon mean-field potential and the schematic separable two-body interaction consistent with it. In this work we have chosen the tetrahedral doubly-closed shell nuclei ^{160}Yb ($Z = 70$ and $N = 90$), ^{110}Zr ($Z = 40$ and $N = 70$) (see also Ref. [31] for this nucleus) and ^{226}Th ($Z = 90$ and $N = 136$) as illustrative examples. We have found out that the characteristic spectra for the totally symmetric representation, i.e. the A_1 irreducible representation of the tetrahedral group T_d, are obtained with the specific sequence composed of 0^+, 3^-, 4^+, 6^+, 6^-, 7^-, 8^+,$\cdots$. These spectra are consistent with those of the simple tetrahedral rotor, although the spectra are more vibrational-like for small deformations. However, it is important to emphasise that only the specific spin-parity combinations appear in the projection calculations in this work in agreement with the group-theory predictions, approaching the rotational pattern closer and closer with increasing tetrahedral deformation.

The Coriolis $|\Delta K| = 1$ mixing is introduced in order to break the time-reversal invariance and to obtain more reliable estimate of moment of inertia; only the slope of energy-vs.-spin relation changes and the qualitative features are not affected by this mixing. It has been also checked that the results of projected spectra are independent of the tilting angle of the cranking axis, which is consistent with the picture that the tetrahedral rotor possesses a 'spherically-symmetric tensor of inertia'.

Stable rigid-rotor energy dependence [$\propto I(I+1)$] appears for larger deformations in the range studied in this article, but an approximately linear dependence is obtained with

decreasing deformations. This transition between the vibrational-like and the rotational pattern occurs at smaller deformation for nuclei with larger mass number. The moment of inertia for the tetrahedral shape increases with increasing deformation, but it is much smaller than the rigid-body value irrespective of the pairing correlations. The impact of the pairing seems rather limited for tetrahedral deformed nuclei at least for the doubly-closed shell nuclei, with relatively large single-particle energy-gaps.

In this work, we have concentrated on the lowest-energy rotational sequences and shown by the calculations that their properties resemble the ones characteristic for the totally symmetric, the so-called A_1 irreducible representation of the tetrahedral point-group, T_d, believed to be characteristic for the lowest-energy sequence of states in fully paired even-even nuclei. From the group theoretical consideration, it is expected that the other irreducible representations, i.e., A_2, E and/or F_1, F_2, would appear in the excited rotational bands of even-even nuclei, see the results of Ref. [31], or in the spectra for odd-odd nuclei. Moreover, there exist different types of representations associated with the so-called double tetrahedral group, specific for the odd nuclei, see Appendix.

We believe that both the experimental analysis as well as the theoretical calculations of the discussed spectral properties will need to include more levels in the future. For this purpose the remaining irreducible representations of the symmetry group may need to be studied compared to the scalar representations that we focused on in this article. The analysis of the irreducible representation structure of the solutions is important for the next step of the analysis, which would consist in calculating the electromagnetic transitions and the branching ratios, the observables which change rapidly with symmetry of the system. This step of the analysis will be essential for establishing the experimental criteria of determining the presence of tetrahedral symmetry in the physics of subatomic systems.

ACKNOWLEDGEMENTS

We appreciate fruitful discussions with Masayuki Matsuo especially on the content of Appendix. This work is supported in part by Grant-in-Aid for Scientific Research (C) No. 22540285 from Japan Society for the Promotion of Science.

Appendix: Spin-parity relations in a tetrahedrally symmetric rotor

Although it may be considered a textbook matter, some spin-parity properties of the rotational energies of the tetrahedrally symmetric rotor will be summarised in this Appendix, to facilitate the comparison between the results of the microscopic calculations with the projection techniques as obtained in this article and the group-theory expectations (see e.g. Ref. [48]). The representation of the rotor states with definite spin-parity $I\pi$ ($\pi = \pm$), $D^{(I\pi)}$, which have a certain symmetry governed by a group G, can be decomposed into its irreducible representations, D_i ($i = 1, \cdots, M$), with multiplicity $a_i^{(I\pi)}$;

$$D^{(I\pi)} = \sum_{i=1}^{M} a_i^{(I\pi)} D_i. \tag{A.1}$$

The multiplicity can be calculated by the standard formula [48],

$$a_i^{(I\pi)} = \frac{1}{N_G} \sum_{R \in G} \chi_{I\pi}(R) \chi_i(R) = \frac{1}{N_G} \sum_{\alpha=1}^{M} g_\alpha \chi_{I\pi}(R_\alpha) \chi_i(R_\alpha), \tag{A.2}$$

where the number N_G is the order of the group G, $\chi_{I\pi}(R)$ and $\chi_i(R)$ are the characters of the representations $D^{(I\pi)}$ and D_i, respectively, for the group element R, and the quantity g_α denotes the number of elements in the class α, whose representative element is R_α. Note that the decomposition (A.1) is performed by a unitary transformation in the $(2I + 1)$ dimensional space of the rotor wave functions for given $I\pi$; more precisely, a specific combination of the K-mixing generates each irreducible representation.

T_d	E	$C_3(8)$	$C_2(3)$	$\sigma_d(6)$	$S_4(6)$
A_1	1	1	1	1	1
A_2	1	1	1	-1	-1
E	2	-1	2	0	0
$F_1(T_1)$	3	0	-1	-1	1
$F_2(T_2)$	3	0	-1	1	-1

TABLE V: Character table for the tetrahedral group T_d. Taken from Ref. [48] (note that $C_2 = S_4^2$ and $F_{1,2}$ are sometimes denoted as $T_{1,2}$).

I^+	0^+	1^+	2^+	3^+	4^+	5^+	6^+	7^+	8^+	9^+	10^+	11^+	12^+	13^+	14^+	15^+	16^+
A_1	1	0	0	0	1	0	1	0	1	1	1	0	2	1	1	1	2
A_2	0	0	0	1	0	0	1	1	0	1	1	1	1	1	1	2	1
E	0	0	1	0	1	1	1	1	2	1	2	2	2	2	3	2	3
$F_1(T_1)$	0	1	0	1	1	2	1	2	2	3	2	3	3	4	3	4	4
$F_2(T_2)$	0	0	1	1	1	1	2	2	2	2	3	3	3	3	4	4	4

I^-	0^-	1^-	2^-	3^-	4^-	5^-	6^-	7^-	8^-	9^-	10^-	11^-	12^-	13^-	14^-	15^-	16^-
A_1	0	0	0	1	0	0	1	1	0	1	1	1	1	1	1	2	1
A_2	1	0	0	0	1	0	1	0	1	1	1	0	2	1	1	1	2
E	0	0	1	0	1	1	1	1	2	1	2	2	2	2	3	2	3
$F_1(T_1)$	0	0	1	1	1	1	2	2	2	2	3	3	3	3	4	4	4
$F_2(T_2)$	0	1	0	1	1	2	1	2	2	3	2	3	3	4	3	4	4

TABLE VI: The number of states $a_i^{(I\pi)}$ belonging to the five irreducible representations of T_d for integer spins; those for each parity are separately shown.

The T_d group has five irreducible representations and classes, whose representative elements are E, $C_2\,(=S_4^2)$, C_3, σ_d, and S_4; see Ref. [48] for the notation. The characters for each irreducible representation are listed in Table V for completeness, and those for the rotor representation [49] are as follows;

$$\chi_{I\pi}(E) = 2I+1, \quad \chi_{I\pi}(C_n) = \sum_{K=-I}^{I} e^{\frac{2\pi K}{n}i} = \frac{\sin\frac{(2I+1)\pi}{n}}{\sin\frac{\pi}{n}}, \tag{A.3}$$

$$\chi_{I\pi}(\sigma_d) = \pi \times \chi_{I\pi}(C_2), \quad \chi_{I\pi}(S_4) = \pi \times \chi_{I\pi}(C_4). \tag{A.4}$$

Combination of the characters in Eqs. (A.3)−(A.4) and in Table V with the formula (A.2) leads to the multiplicities, $a_i^{(I\pi)}$, which are summarised in Table VI for integer spins up to $I = 16$. It is easy to verify that $a_{A_1}^{(I\pm)} = a_{A_2}^{(I\mp)}$, $a_E^{(I+)} = a_E^{(I-)}$, and $a_{F_1}^{(I\pm)} = a_{F_2}^{(I\mp)}$. In the table, $a_i^{(I\pi)} = 0$ means that such states are not allowed, and $a_i^{(I\pi)} = 2$ means that states are doubly degenerate. In this way the characteristic spin-parity for the A_1 representation in Eq. (16) follows.

T_d^D	E		$C_3(8)$		$C_2(3)$	$\sigma_d(6)$	$S_4(6)$	
$E_{1/2}(E_1')$	2	-2	1	-1	0	0	$\sqrt{2}$	$-\sqrt{2}$
$E_{5/2}(E_2')$	2	-2	1	-1	0	0	$-\sqrt{2}$	$\sqrt{2}$
$G_{3/2}(G')$	4	-4	-1	1	0	0	0	0

TABLE VII: Character table specific for the extended (also called 'double') tetrahedral group T_d^D. The second entry in the corresponding columns denotes the characters of extended elements. [Taken from Ref. [39] (note that $E_{1/2}$, $E_{5/2}$ and $G_{3/2}$ are sometimes denoted as E_1', E_2' and G').]

I^+	$\frac{1}{2}^+$	$\frac{3}{2}^+$	$\frac{5}{2}^+$	$\frac{7}{2}^+$	$\frac{9}{2}^+$	$\frac{11}{2}^+$	$\frac{13}{2}^+$	$\frac{15}{2}^+$	$\frac{17}{2}^+$	$\frac{19}{2}^+$	$\frac{21}{2}^+$	$\frac{23}{2}^+$	$\frac{25}{2}^+$	$\frac{27}{2}^+$	$\frac{29}{2}^+$	$\frac{31}{2}^+$
$E_{1/2}(E_1')$	1	0	0	1	1	1	1	1	2	2	1	2	3	2	2	3
$E_{5/2}(E_2')$	0	0	1	1	0	1	2	1	1	2	2	2	2	2	3	3
$G_{3/2}(G')$	0	1	1	1	2	2	2	3	3	3	4	4	4	5	5	5

I^-	$\frac{1}{2}^-$	$\frac{3}{2}^-$	$\frac{5}{2}^-$	$\frac{7}{2}^-$	$\frac{9}{2}^-$	$\frac{11}{2}^-$	$\frac{13}{2}^-$	$\frac{15}{2}^-$	$\frac{17}{2}^-$	$\frac{19}{2}^-$	$\frac{21}{2}^-$	$\frac{23}{2}^-$	$\frac{25}{2}^-$	$\frac{27}{2}^-$	$\frac{29}{2}^-$	$\frac{31}{2}^-$
$E_{1/2}(E_1')$	0	0	1	1	0	1	2	1	1	2	2	2	2	2	3	3
$E_{5/2}(E_2')$	1	0	0	1	1	1	1	1	2	2	1	2	3	2	2	3
$G_{3/2}(G')$	0	1	1	1	2	2	2	3	3	3	4	4	4	5	5	5

TABLE VIII: The number of states $a_i^{(I\pi)}$ belonging to the three irreducible representations specific for T_d^D for half-odd integer spins; those for each parity are separately shown.

As for the excitations of odd nuclei, i.e., for half-odd integer spins I, the same calculation can be done, but one has to consider the extended rotation group (the double group) G^D, see e.g. Ref. [39] (or equivalently, the two-valued representations [48]). In the extended group, the number of elements is doubled by extending the range of rotational angle about an axis from 2π to 4π, because the 2π rotation is not the identity operation but changes sign for the rotor states with half-integer spins. The character table specific for the double tetrahedral group T_d^D is shown in Table VII, and the resultant multiplicities are given in Table VIII, where $a_{E_{1/2}}^{(I\pm)} = a_{E_{5/2}}^{(I\mp)}$ and $a_{G_{3/2}}^{(I+)} = a_{G_{3/2}}^{(I-)}$ can be easily confirmed. Table VIII can be also used to see how a spherical single-particle orbit j^π decomposes

into the two-fold ($E_{1/2,\,5/2}$) and four-fold ($G_{3/2}$) degenerate orbits for finite tetrahedral deformation.

---

[1] A. Bohr and B. R. Mottelson, *Nuclear Structure*, Vol. II Benjamin, New York (1975).

[2] P. Ring and P. Schuck, *The Nuclear Many-Body Problem*, Springer, New York (1980).

[3] J. Dudek, A. Góźdź, K. Mazurek and H. Molique, J. Phys. G **37** (2010), 064032.

[4] J. Dudek, A. Góźdź, N. Schunck and M. Miśkiewicz, Phys. Rev. Lett. **88**, 252502 (2002).

[5] N. Onishi and R. K. Sheline, Nucl. Phys. A **165**, 180 (1971).

[6] D. Robson, Nucl. Phys. A **308**, 381 (1978).

[7] D. Robson, Phys. Rev. Lett. **42**, 876 (1979).

[8] D. Robson, Phys. Rev. C **25**, 1108 (1982).

[9] X. Li and J. Dudek, Phys. Rev. **C49**, R1250 (1994).

[10] S. Takami, K. Yabana and M. Matsuo, Phys. Lett. B **431**, 242 (1998).

[11] M. Matsuo, S. Takami and K. Yabana, in the proceedings of "Nuclear Structure 98", Gatlinburg, Tennessee, Aug., 1998, AIP Conference Proceedings 481, p. 345.

[12] M. Yamagami, K. Matsuyanagi and M. Matsuo, Nucl. Phys. A **693**, 579 (2001).

[13] P. Olbratowski, J. Dobaczewski, P. Powałowski, M. Sadziak and K. Zberecki, Int. J. Mod. Phys. E **15**, 333 (2006).

[14] K. Zberecki, P. Magierski, P.-H. Heenen and N. Schunck, Phys. Rev. C **74**, 051302(R) (2006).

[15] Y.-S. Chen, Y. Sun and Z.-C. Gao, Phys. Rev. C **77**, 061305(R) (2008).

[16] K. Zberecki, P.-H. Heenen and P. Magierski, Phys. Rev. C **79**, 014319 (2009).

[17] K. Hara and Y. Sun, Int. J. Mod. Phys. E **4**, 637 (1995).

[18] K. Hara, A. Hayashi and P. Ring, Nucl. Phys. **A385**, 14 (1982).

[19] K. Enami, K. Tanabe and N. Yoshinaga, Phys. Rev. C **59**, 135 (1999).

[20] S. Tagami and Y. R. Shimizu, Prog. Theor. Phys. **127**, 79 (2012).

[21] L. M. Robledo, Phys. Rev. C **79**, 021302(R) (2009).

[22] S. Ćwiok, J. Dudek, W. Nazarewicz, J. Skalski and T. Werner, Comp. Phys. Comm. **46**, 379 (1987).

[23] N. Tajima, Y. R. Shimizu and S. Takahara, Phys. Rev. C **82**, 034316 (2010).

[24] J. Dudek, Z. Szymański and T. Werner, Phys. Rev. **C23**, 920 (1981).

[25] J. Dudek and T. Werner, J. Phys. **G 4**, 1543 (1978);

[26] J. Dudek, A. Majhofer, J. Skalski, T. Werner, S. Ćwiok and W. Nazarewicz, J. Phys. **G5**, 1359 (1979).

[27] S. Kahane, S. Raman and J. Dudek, Phys. Rev. C **40**, 2282 (1989).

[28] Z. Lojewski, B. Nerlo-Pomorska, K. Pomorski and J. Dudek, Phys. Rev. C **51**, 601 (1995).

[29] J. Dudek, K. Mazurek, D. Curien, A. Dobrowolski, A. Góźdź, D. Hartley, A. Maj, L. Riedinger and N. Schunck, Acta Phys. Polonica B **40**, 713 (2009).

[30] N. Schunck, J. Dudek, A. Góźdź and P. H. Regan, Phys. Rev. C **69**, 061305(R) (2004).

[31] S. Tagami, Y. R. Shimizu and J. Dudek, Proc. of the YKIS2011 Symposium on *Frontier Issues in Physics of Exotic Nuclei*, Prog. Theor. Phys. Suppl. **196**, 334 (2012).

[32] T. Sumikama, et al., Phys. Rev. Lett. **106**, 202501 (2011).

[33] J. Dudek, A. Góźdź and D. Rosły, Acta Phys. Polonica **32**, 2625 (2001).

[34] J. Dudek, A. Góźdź, D. Curien, V. Pangon and N. Schunck, Acta Phys. Polonica **38**, 1389 (2007).

[35] A. Góźdź, M. Miśkiewicz and J. Dudek, Int. J. Mod. Phys. **E17**, 272 (2008).

[36] M. Miśkiewicz, A. Góźdź and J. Dudek, Int. J. Mod. Phys. **E13**, 127 (2004).

[37] W. Greiner and J. A. Maruhn, *Nuclear Models*, Springer Verlag Berlin Heidelberg New York, 1996.

[38] G. Herzberg, *Molecular Spectra and Molecular Structure* Vol. II, *Infrared and Raman Spectra of Polyatomic Molecules*, Chap. I-3 and IV-3. (D. Van Nostrand Company Inc., New York, 1945).

[39] G. Herzberg, *Molecular Spectra and Molecular Structure* Vol. III, *Electronic Spectra and Electronic Structure of Polyatomic Molecules*, Chap. I-1 and Appendx I. (D. Van Nostrand Company Inc., New York, 1966).

[40] S. Frauendorf, Acta Phys. Polonica B **32**, 2661 (2001).

[41] N. Schunck, J. Dudek and S. Frauendorf, Acta Phys. Polonica B **B36** 1071 (2005).

[42] M. de Voigt, J. Dudek and Z. Szymański, Rev. Mod. Phys. **55** 949 (1983)

[43] M. A. Deleplanque, S. Frauendorf, V. V. Pashkevich, S. Y. Chu and A. Unzhakova, Phys.

Rev. C **69**, 044309 (2004).

[44] K. Mazurek, J. Dudek, A. Gozdz, D. Curien, M. Kmiecik and A. Maj, Acta Phys. Polonica B **40**, 731 (2009).

[45] N. Schunck and J. Dudek, Int. J. Mod. Phys. **E13** 213 (2004).

[46] N. Schunck, P. Olbratowski, J. Dudek and J. Dobaczewski, Int. J. Mod. Phys. **E15**, 490 (2006).

[47] J. Dudek, A. Góźdź and N. Schunck, Acta Phys. Polonica **B34** 2491 (2003)

[48] M. Hamermesh, *Group Theory and Its Application to Physical Problems*, (Dover Publications, Inc., New York, 1962).

[49] E. B. Wilson, J. Chem. Phys. **3**, 276 (1935).